ELECTRODE-EXPANSION MHD IN A PLASMA-FILLED ROD PINCH*

D. Mosher[+], J.W. Schumer, B.V. Weber, and D. Ponce[a]

Plasma Physics Division, Naval Research Laboratory, Washington, DC 20375, USA

Abstract

The Gamble II plasma-filled rod pinch (PFRP) produces an order-of-magnitude higher x-ray dose and smaller FWHM source size than achieved with a vacuum rod pinch. Intense electron deposition at the tip produces a high-energy-density expanding-tungsten plasma, the bremsstrahlung from which creates a low-intensity halo around the source core that increases the effective source size for some applications. The plasma motion has been measured with a holographic interferometer. Using the distribution of electron deposition derived from line-spread measurements, the observations are compared with zero-and one-dimensional self-similar MHD modeling of the plasma motion. Results demonstrate that magnetic-field and ohmic-heating effects during electron deposition are important to understanding PFRP dynamics.

I. INTRODUCTION

The rod-pinch diode is an important new radiography source in the 1-MV and above x-ray regime.[1-5] A standard vacuum rod-pinch on the NRL Gamble II generator [1], consisting of a mm-diam tapered tungsten anode rod protruding through, and a few cm beyond an annular carbon cathode, is characterized by a 30- to 60-Ohm impedance and an x-ray source size comparable to the rod diameter. The plasma-filled rod pinch (PFRP) extends megavolt rod-pinch radiography to low-impedance/high-current generators by surrounding the rod downstream of the cathode with a 10^{16}-cm^{-3} plasma.[6-7] The plasma initially shorts the diode, and then opens to a few-Ohm impedance, concentrating a 0.5-MA, MeV electron beam near the rod tip. The high current density on the tapered tip produces an order-of-magnitude higher x-ray dose (20 rad at 1 m) and smaller FWHM source size than achieved with a vacuum rod pinch on Gamble II.

The intense electron deposition in the PFRP produces a high-energy-density expanding-tungsten plasma, the bremsstrahlung from which creates low-intensity wings around the source core that increases the effective source size for some applications. This two-dimensional, time-dependent tungsten plasma motion has been studied [7] with a holographic interferometer [8]. Using an axial distribution of electron deposition derived from side-viewing (90° to the rod) line-spread measurements [5,9],

these observations are compared with zero- and one-dimensional self-similar MHD modeling of the plasma motion. Simulated 0° (forward on the rod axis) line spreads derived from the zero-dimensional MHD model agree well with measurements. Agreement between the one-dimensional model and Schlieren measurements [7] demonstrates that magnetic-field and ohmic-heating effects during electron deposition are important to understanding the dynamics of the plasma-filled rod pinch.

II. DISCUSSION AND CONCLUSIONS

The experimental configuration has been described elsewhere.[6,7] Here, electrical, Schlieren, interferometry, on-axis and side-viewing rolled-edge measurements for PFRPs with 1-mm-diam tapered-tungsten rods are employed in the analysis. Figure 1 shows the diode current, diode voltage, and bremsstrahlung x-ray traces for a typical shot. Time is measured from the start of the x-ray pulse, when voltage first appears at the rod tip. Negative times correspond to the run-down phase during which the injected plasma is displaced by **J×B** forces, sweeping open a vacuum gap along the rod.[6,7] Voltage at negative times is then associated with $d(LI)/dt$, where L is the inductance associated with the evolving vacuum gap. Using the variations of V and I shown in Fig. 1, L is calculated to be close to linearly rising from the start of the current pulse, reaching 22 nH at t = 0. This variation
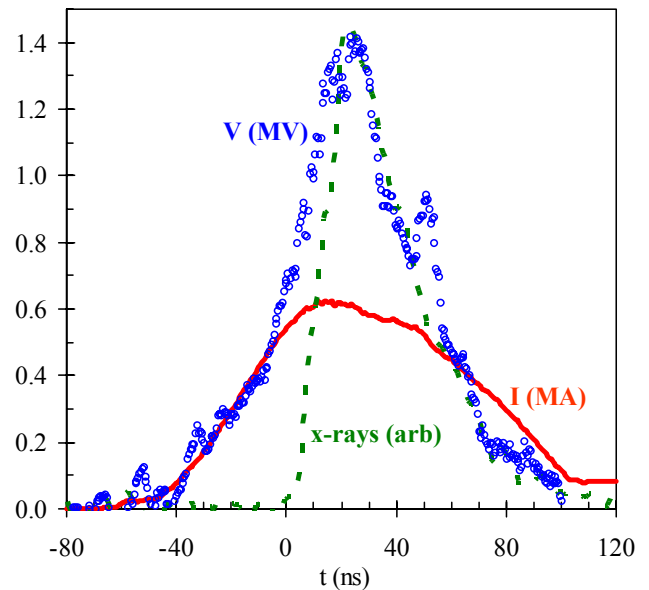

Figure 1. Diode voltage, current, and x-ray traces.

Report Documentation Page		*Form Approved* *OMB No. 0704-0188*

1. REPORT DATE **JUN 2003**	2. REPORT TYPE **N/A**	3. DATES COVERED **-**	
4. TITLE AND SUBTITLE **Electrode-Expansion Mhd In A Plasma-Filled Rod Pinch**		5a. CONTRACT NUMBER	
		5b. GRANT NUMBER	
		5c. PROGRAM ELEMENT NUMBER	
6. AUTHOR(S)		5d. PROJECT NUMBER	
		5e. TASK NUMBER	
		5f. WORK UNIT NUMBER	
7. PERFORMING ORGANIZATION NAME(S) AND ADDRESS(ES) **Plasma Physics Division, Naval Research Laboratory, Washington, DC 20375, USA**		8. PERFORMING ORGANIZATION REPORT NUMBER	
9. SPONSORING/MONITORING AGENCY NAME(S) AND ADDRESS(ES)		10. SPONSOR/MONITOR'S ACRONYM(S)	
		11. SPONSOR/MONITOR'S REPORT NUMBER(S)	

12. DISTRIBUTION/AVAILABILITY STATEMENT
Approved for public release, distribution unlimited

13. SUPPLEMENTARY NOTES
See also ADM002371. 2013 IEEE Pulsed Power Conference, Digest of Technical Papers 1976-2013, and Abstracts of the 2013 IEEE International Conference on Plasma Science. IEEE International Pulsed Power Conference (19th). Held in San Francisco, CA on 16-21 June 2013. U.S. Government or Federal Purpose Rights License, The original document contains color images.

14. ABSTRACT
The Gamble II plasma-filled rod pinch (PFRP) produces an order-of-magnitude higher x-ray dose and smaller FWHM source size than achieved with a vacuum rod pinch. Intense electron deposition at the tip produces a high-energy-density expanding-tungsten plasma, the bremsstrahlung from which creates a low-intensity halo around the source core that increases the effective source size for some applications. The plasma motion has been measured with a holographic interferometer. Using the distribution of electron deposition derived from line-spread measurements, the observations are compared with zero-and one-dimensional self-similar MHD modeling of the plasma motion. Results demonstrate that magnetic-field and ohmic-heating effects during electron deposition are important to understanding PFRP dynamics.

15. SUBJECT TERMS

16. SECURITY CLASSIFICATION OF:			17. LIMITATION OF ABSTRACT	18. NUMBER OF PAGES	19a. NAME OF RESPONSIBLE PERSON
a. REPORT **unclassified**	b. ABSTRACT **unclassified**	c. THIS PAGE **unclassified**	**SAR**	**4**	

Standard Form 298 (Rev. 8-98)
Prescribed by ANSI Std Z39-18

corresponds to the opening of a cylindrical volume around the rod with a 1.2-cm radius and length increasing from 0 to 3 cm during the run-down. For t > 0, the voltage at the tip V_{tip} is then given by $V - 2.2 \times 10^{-8} dI/dt$, so that the electron-beam power heating the full 3-cm length of the rod is taken to be IV_{tip} in the analysis.

Figure 2 compares Schlieren images of vacuum (50-kA) and plasma-filled (500-kA) rod pinches 60 to 70 ns after the start of x-radiation. The image scales are identical and the rod tips are aligned (initial rod image shown for the PFRP). For the PFRP, high-energy-density tungsten plasma expands from the tip during bremsstrahlung emission, creating a low-intensity halo around the x-ray-source core that is manifested as extended wings in the on-axis line spread (Fig. 3). Also shown in Fig. 2 is the PFRP 90° line spread demonstrating that time-integrated e-beam deposition along the rod correlates with the observed plasma expansion.
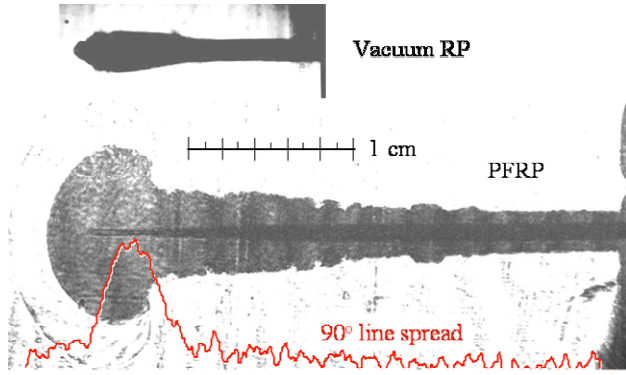

Figure 3. PFRP edge- and line-spread functions at 0°.

Figure 3 shows typical 0° edge- and line-spread functions for the PFRP that have two distinct spot-size scales. The 0.4-mm FWHM is consistent with the 90° line-spread distribution of Fig. 2 showing concentration of electron deposition on the tapered tip. The 1.7-mm LLNL definition source size [1] reflects the extended line-spread wings of Fig. 3, which, in turn, reflect the observed rod-plasma expansion of Fig. 2.

The zero-dimensional MHD analysis seeks to explain the observed line-spread wings by assuming a cylindrical self-similar expansion of plasma from the tapered tip. A Gaussian tungsten-density distribution n(r,t) of width R(t) is assumed.

$$n(r,t) = \frac{N}{\pi R^2(t)} exp\left(-r^2 / R^2\right) \quad (1)$$

Here, N(1/cm) is the fixed line density given by

$$N = \frac{\pi}{3 m_W} R_b^2 \rho_0 \quad , \quad (2)$$

m_W is the mass of a tungsten ion, ρ_0 is the solid rod mass density, $R_b = L/20$ is the radius of a cone of rod-tip length L assumed to be heated by the e-beam. Based on Fig. 2, L ≈ 3-4 mm is reasonable. The continuity equation is then
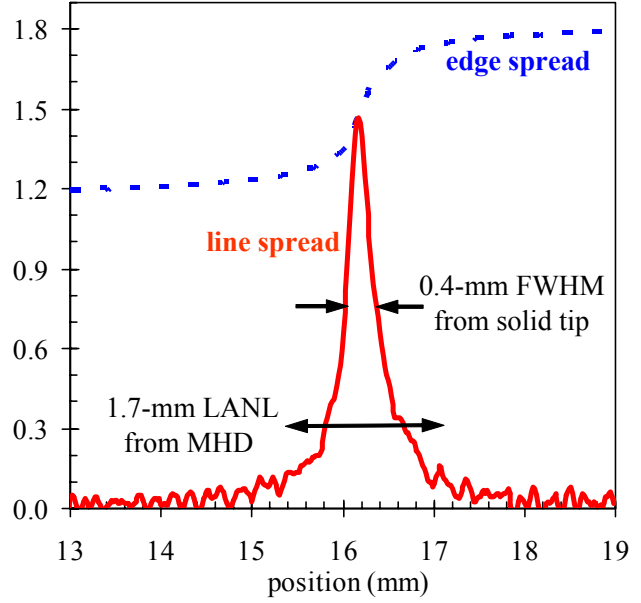

Figure 2. Schlieren images for vacuum and plasma-filled RPs 60-70 ns after start of x-ray emission.

satisfied when the radial fluid velocity takes the form

$$v(r,t) = \frac{r}{R(t)} \frac{dR}{dt} \quad . \quad (3)$$

Substituting these forms into the fluid equation of motion,

$$\frac{d^2 R}{dt^2} = \frac{2(1 + Z)kT}{m_W R} \quad , \quad (4)$$

where T(t) is the temperature and Z(T) is the ionization level. Temperature is determined from radially-integrated energy balance per unit length given by

$$E_{int}(t) = \int_0^t \left(P_h - \varepsilon\sigma T^4 \cdot 2\pi R\right) dt - \frac{m_W N}{2}\left(\frac{dR}{dt}\right)^2 . \quad (5)$$

In Eq. (5), E_{int} is the internal energy, the last term represents kinetic energy, P_h is the beam-heating power and black-body-like radiation P_{bb} from the characteristic radius R is assumed. The quantities $T(E_{int})$ and Z(T) are determined from SESAME [10] equation-of-state data for tungsten. Measured x-ray dose from the rod tip [6] indicates that $P_h = IV_{tip}/3L$ is appropriate; a piece-wise linear fit to it is used to solve Eqs. (4) and (5). Note that L and emissivity ε are free parameters.

Figure 4 shows solutions of the above equations for ε = 0.3 and two values of L = 3 and 4 mm. For each trace, the smaller value of L yields the upper curve. The single P_h curve is for L = 4 mm; that for 3 mm is 4/3 larger. At peak temperature, Z in the 14 to 16 range is calculated. Of greatest interest here is R(t) as it determines the wings of the 0° line spread. This radius is found to depend weakly on ε in the range 0.03 to 0.3. At each instant, the bremsstrahlung radiation $P_{br}(r,t)$ is assumed to scale like $IV_{tip}^{3/2}$ in time with a radial dependence proportional to n(r,t) of Eq. (1). Integrating P_{br} in time over the power pulse then provides the 0° point spread function PS(r) used to calculate the line spread function LS(y) in Eq. (6).
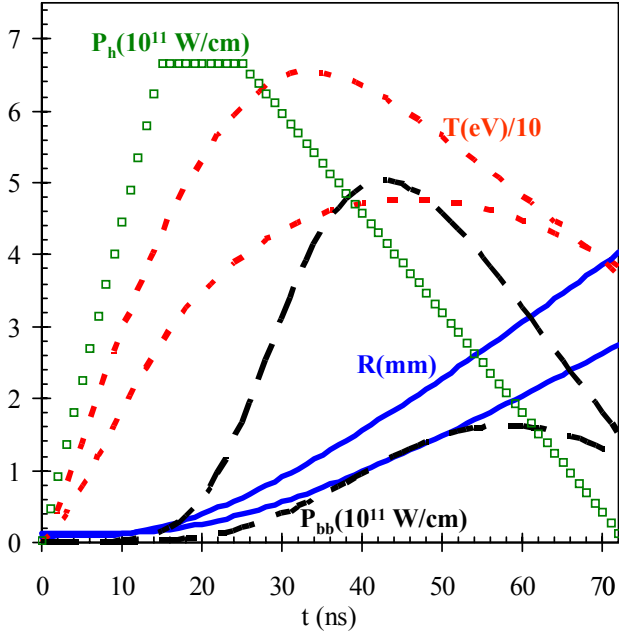
Figure 4. Zero-dimensional tungsten-plasma evolution for L = 3 mm (upper) and L = 4 mm (lower).

$$LS(y) = \int_y^\infty \frac{PS(r)rdr}{\sqrt{r^2 - y^2}} \qquad (6)$$

Figure 5 compares calculated line spreads for L = 3 and 4 mm with that measured in Fig. 3. Results for ε = 0.03 are indistinguishable from those of Fig. 5 for ε = 0.3. These good fits to the measurements using L values consistent with tip deposition from the 90° line spread (Fig. 2) confirm that PFRP tip expansion is the source of the extended wings observed on the 0° line spread.
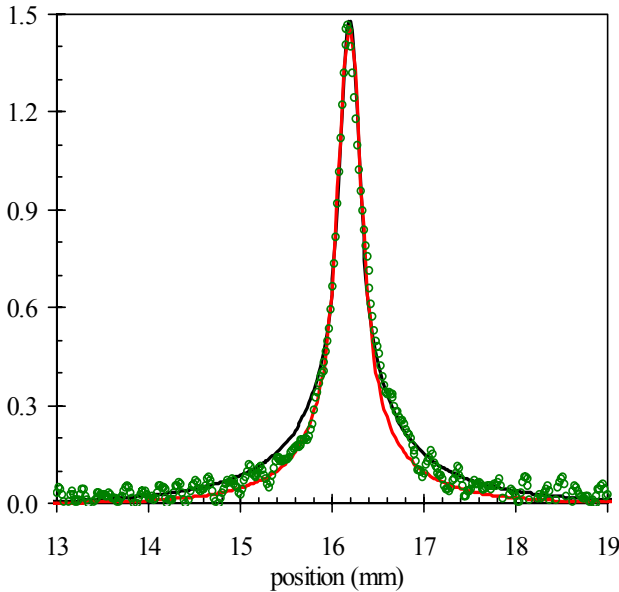

Figure 5. Measured (points) and predicted (solid) 0° line spreads for L = 3 mm (upper curve) and L = 4 mm (lower curve).

The ability of the zero-dimensional model to predict tip expansion is demonstrated by the fits of Fig. 5, and consistency between the values of R(t) at 70 ns in Fig. 4 with the Fig. 2 Schlieren boundary at the tip. It is desired to extend the analysis to a one-dimensional axial self-similar model in order to better understand rod-plasma expansion away from the tip. Equation (1) is generalized to include the axial variation of line density associated with the local solid-density rod radius.

$$N(z) = \pi R_{rod}^2(z)\rho_0 / m_W \qquad (7)$$

Local rod heating $P_{hz}(z,t)$ follows the 90° line spread of Fig. 2 in space and IV_{tip} in time. The local beam current density $J_{br}(z,t)$ entering the rod plasma follows this line spread in space and I in time. Conservation of charge requires that the axial return current in the rod $I_z(z,t)$ is

$$I_z = 2\pi \int_0^z J_{br}(z',t)rdz' \qquad , \qquad (8)$$

which is therefore proportional to the 90° edge spread.

With the addition of magnetic pressure, Eq. (4) is modified to

$$\frac{d^2 R(z)}{dt^2} = \frac{2}{m_W R}\left[(1+Z)kT - \frac{I_z^2}{200N}\right] \qquad (9)$$

in cgs units except for I_z in A. Energy-balance now takes the form

$$E_{int}(t) = \int_0^t \left(P_{hz} - P_{bb} + 7.4 \times 10^6 \frac{\eta(T)I_z^2}{2\pi R^2} - \frac{I_z^2}{100R}\frac{dR}{dt}\right) dt$$
$$- \frac{m_W N}{2}\left(\frac{dR}{dt}\right)^2 \qquad , \qquad (10)$$

where η(Ohm-cm) is the Spitzer resistivity. The ohmic heating and work on the plasma in Eq. (10) derive from the radial dependence of return-current density that preserves self-similarity in Eq. (9), i.e., $j_z \times B_\theta \sim n(r,t)$.

$$j_z(r,z,t) = \frac{I_z(z,t)}{2\pi R^2}\frac{d}{udu}\left[1 - (1+u^2)exp(-u^2)\right]^{1/2} \quad (11)$$

In Eq. (11), $u = r/R(z,t)$. The self-similar axial-current density resembles a Gaussian with characteristic radius 1.2R. Note that formally, Eqs. (8)-(10) are only valid for $dR/dz << 1$, so that results near the rod tip are suspect.

Figure 6 shows the applied axial variations of line density, beam heating and return current, and the computed R(z) at 110 ns from the solution of Eqs. (9) and (10). For z < 0.6 cm, beam heating of the rod plasma dominates over ohmic heating, and magnetic pressure is much less than kinetic pressure, so that the zero-dimensional model can be employed. For larger values of z, axial-return current has accumulated to high values and temperature is lower due to reduced beam deposition and higher mass. Under these conditions, ohmic heating dominates and magnetic pressure retards plasma expansion, so that the return-current effects in the one-dimensional model are
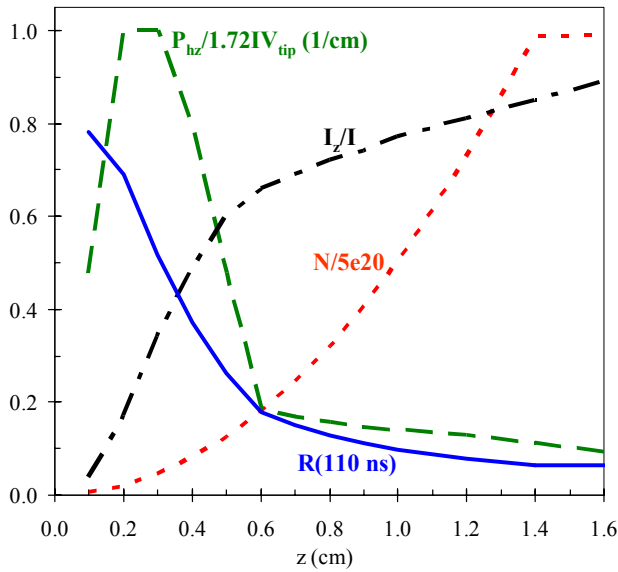
Figure 6. One-dimensional model-input variations vs axial position and resulting radius at 110 ns.

important. These effects result in the observed sharp Schlieren-boundary transition between the two regions.

Figure 7 shows a shadow of the initial rod superimposed on Schlieren and interferometry images at 110 ns, the end of the power pulse.[6,7] In order to relate R(z) from the one-dimensional model (Fig. 6) to the measurements, the electron density at the Schlieren boundary has been determined by fringe counting and Abel inversion. This electron density, about 4×10^{18} cm^{-3}, is set equal to Zn(r,R) using computed Z and R values at 110 ns and various axial positions. Solving for r then yields the computed Schlieren boundary as a function of z. The results of this calculation are also shown in Fig. 7. Fair agreement between the measured and computed Schlieren boundaries demonstrate the importance of return-current and magnetic-field effects to the rod-plasma expansion dynamics behind the rod tip.
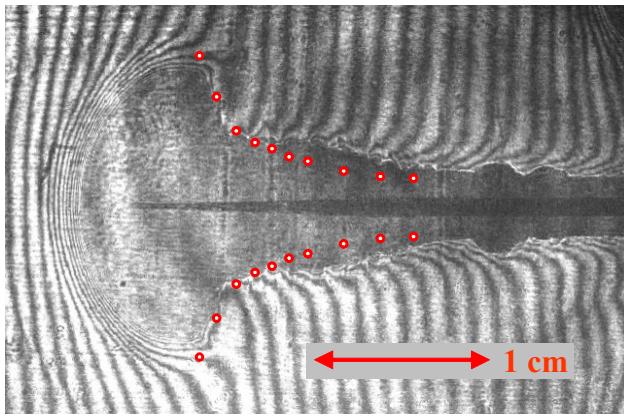

Figure 7. Schlieren, interferometry, initial-rod images, and computed Schlieren boundary (circles) at 110 ns.

In conclusion, measured Schlieren images and line-spread distributions compare well with simple zero- and one-dimensional self-similar MHD modeling of tungsten-plasma expansion for the plasma-filled rod pinch. Close to the tip, beam heating of the rod plasma and kinetic pressure dominate the dynamics so that the zero-dimensional model can be employed to estimate how expansion alters the radiographic source. Behind the tip, accumulated axial-return current and reduced beam deposition lead to high ohmic heating and a magnetic pressure sufficient to retard plasma expansion, so that the more sophisticated analysis is required.

Future plans include 2-dimensional MHD and particle-in-cell (PIC) simulations of the PFRP. Challenges for this objective will be to model: rod return-current-heating effects during the run-down phase, effects of adsorbed gases in the rod, a self-consistent transition between run-down and plasma-opening phases, and beam- and plasma-current distributions in the expanding-rod plasma after opening. It is hoped that additional modeling will help in the development of geometries that reduce the MHD wings in the line spread to enhance the radiographic applications of the plasma-filled rod pinch.

III. REFERENCES

[1] R.J. Commisso, et al., "Experimental evaluation of a megavolt rod-pinch diode as a radiography source," IEEE Trans. Plasma Sci. **30**, 338-350(2002), and references therein.

[2] F.C. Young, et al., "Rod Pinch Diode Operation at 2 to 4 MV for High Resolution Pulsed Radiography," Phys. Plasmas **9**, 4815-4818(2002).

[3] G. Cooperstein, et al., "Theoretical modeling and experimental characterization of a rod-pinch diode," Phys. Plasmas **8**, 4618-4636(2001).

[4] R.J. Commisso, et al., "Characterization of the Rod-Pinch Diode at 2 to 4 MV as a High-Resolution Source for Flash Radiography," AIP Conf. Proc **650**, pp. 183-186.

[5] F. Bayol, et al., F.C. Young, et al., and D. Mosher, et al., these proceedings.

[6] B.V. Weber, et al., "The Plasma-Filled Rod-Pinch Diode: a New Technique to Concentrate MeV Electron Beams to Ultra-High Power- and Energy-Densities," AIP Conf. Proc **650**, 2002, pp. 191-194.

[7] D. Ponce, et al., these proceedings.

[8] Installed at NRL by J. Moschella and C. Vidoli, HY-Tech Research Corp.

[9] D. Mosher, et al., "An Electron-Beam-Heating Model for the Gamble II Rod Pinch," AIP Conf. Proc **650**, 2002, pp. 199-202.

[10] K.S. Holian, Ed., T-4 Handbook of Material Properties Data Book, Vol. 1c: EOS. Los Alamos National Laboratory, Nov. 1984.